ICARUS 59, 41–59 (1984)

Bidirectional Reflectance Spectroscopy

3. Correction for Macroscopic Roughness

BRUCE HAPKE

Department of Geology and Planetary Science, University of Pittsburgh, Pittsburgh, Pennsylvania 15260

Received August 2, 1982; revised March 13, 1984

A mathematically rigorous formalism is derived by which an arbitrary photometric function for the bidirectional reflectance of a smooth surface may be corrected to include effects of general macroscopic roughness. The correction involves only one arbitrary parameter, the mean slope angle $\bar{\theta}$, and is applicable to surfaces of any albedo. Using physically reasonable assumptions and mathematical approximations the correction expressions are evaluated analytically to second order in $\bar{\theta}$. The correction is applied to the bidirectional reflectance function of B. Hapke (1981, *J. Geophys. Res.* **86**, 3039–3054). Expressions for both the differential and integral brightnesses are obtained. Photometric profiles on hypothetical smooth and rough planets of low and high albedo are shown to illustrate the effects of macroscopic roughness. The theory is applied to observations of Mercury and predicts the integral phase function, the apparent polar darkening, and the lack of limb brightness surge on the planet. The roughness-corrected bidirectional reflectance function is sufficiently simple that it can be conveniently evaluated on a programmable hand-held calculator.

I. INTRODUCTION

In an earlier paper (Hapke, 1981) expressions were derived which describe the bidirectional reflectance from a macroscopically smooth, particulate surface, and which also relate the single scattering albedo of a surface particle to the absorption coefficient of the material. The reflectance function takes account of multiple scattering and interparticle shadowing. In a companion to that paper (Hapke and Wells, 1981) it was demonstrated by comparison of predictions from this function with results of laboratory experiments and astronomical observations that the function can be used to measure quantitiatively the spectral absorption coefficient of a powder and predict the brightness profiles on planetary surfaces.

The only major discrepancies between observations and this theory occur near the poles and illuminated limb of a low albedo planet. Rigorous solutions of the radiative transfer equation for macroscopically smooth, dark surfaces (Chandrasekhar, 1960; Hapke, 1963, 1981) imply that, when single scattering dominates, the brightness should be independent of latitude and highly peaked at the illuminated limb. These predictions are contrary to observations (Hapke, 1966, 1977). Previously it had been assumed that these discrepancies are due to roughness and could be removed if this factor could be taken into account properly.

There have been relatively few attempts in the literature to treat the effects of macroscopic roughness on planetary photometric functions, and most of these have dealt with specific topographic shapes. Van Diggelen (1959) and Hameen-Anttila (1967) considered the effects of cup-shaped depressions. Hapke (1966) used a model for the Moon in which the surface is taken to be covered with cylindrical troughs whose axes are parallel to meridians of longitude. The latter treatment is unsatisfactory in several respects. First, the geometry is highly artificial. Second, only single scattering is taken into account. Third, in common with most models which treat specific

0019-1035/84 $3.00

shapes, the reflectance has several different forms, depending on the angles involved, and is cumbersome to use.

Cook (1981) has developed a lunar photometric function which includes roughness effects. While his function has the advantage of being mathematically simple, it is based on an empirical psuedo-Lambertian formalism, rather than the radiative transfer equation. Lumme and Bowell (1981a,b) have recently published a rough-surfaced scattering model. However, there appear to be serious errors in their photometric function (Hapke, 1982). Among the many difficulties with their treatment are the following: (1) The roughness is assumed to have no effect on the multiply-scattered component of light. This is physically impossible and violates the principle of conservation of energy. (2) Their roughness correction makes the reflectance approach zero at the limb. Thus, low albedo bodies, such as the Moon, should be strongly limb darkened, contrary to observations. While it may be possible to fit some astronomical data to their theory, the relations between the deduced photometric parameters and actual surface properties of the body are unclear and are likely to be seriously in error.

There is a considerable body of literature which discusses shadowing on a randomly rough surface; e.g., Muhleman (1964), Wagner (1967), Saunders (1967), and Hagfors (1968) and references cited therein. Most of these papers deal with specularly reflecting facets, usually in connection with either analyses of sea glitter or the special case of backscatter for radar applications. None of the references with which I am familiar adequately treat the major problems of effective surface tilt nor the correlation between the illumination and viewing shadows at small azimuth angles.

It is the purpose of this paper to derive an expression which can be used to correct any general bidirectional reflectance function of a smooth surface for effects of roughness of arbitrary topology.

II. COORDINATE SYSTEMS

In general, any bidirectional reflectance expression is a function of three independent angular variables. Frequently these are taken to be the zenith angle of the incident ray i, the zenith angle of the exit ray e, and the azimuth angle ψ, which is the angle between the projections onto the surface of the incident and exit rays. In planetary problems the phase angle g is often used instead of the azimuth angle because when analyzing the image of a planet, g is constant over the entire image.

For many planetary applications it is convenient to use luminance coordinates, in which the independent variables are the luminance longitude Λ, luminance latitude L, and phase angle g. In this coordinate system the equator is the great circle on the planet containing the subsolar and subobserver points; the central meridian contains the subobserver point; positive longitude is to the east; and the phase angle is positive when the subsolar point is to the west of the subobserver point.

These coordinate systems are related by the following equations:

$$\cos e = \cos \Lambda \cos L, \tag{1}$$

$$\cos i = \cos(\Lambda + g) \cos L, \tag{2}$$

$$\cos \Psi = (\cos g - \cos i \cos e)/\sin i \sin e, \tag{3}$$

where $0 \leq \Psi \leq \pi$.

III. ASSUMPTIONS AND APPROACH

The following assumptions are made:

(1) All relevant objects are large compared to the wavelength of light so that geometrical optics is applicable.

(2) The mean slope $\bar{\theta}$ is assumed to be reasonably small. Scarps and overhangs with slopes greater than $\pi/2$ constitute a negligible part of the surface. Although the general roughness correction will be derived for an arbitrary slope distribution, the

resulting expressions are greatly simplified if powers of $\bar{\theta}$ greater than 2 can be ignored.

(3) Multiple scattering of light from one macroscopic surface facet to another is neglected. This assumption is consistent with the second. For example, it is straightforward to show that the light scattered from the insides of a hollow spherical cup of maximum slope θ_M, covered by a Lambert surface of normal albedo A_N, onto the central facet at the bottom when the cup is illuminated vertically by light of intensity J is $(J/4)A_N \sin^2\theta_M$. Thus, the ratio of once-scattered to incident illumination is second order in slope and can be ignored if the slopes and/or the albedo are small.

(4) It is assumed that the surface is made up of facets tilted at a variety of angles which have no preferred direction in azimuth but can be described by a Gaussian distribution in zenith angle. The assumption of azimuth independence will certainly be true on the average for surfaces covered by craters, boulders, hills, and similar features, and it also appears to be true for the surface of the ocean (Cox and Munk, 1954). Thus, it is probably a reasonable approximation for most of the bodies in the solar system. Its validity may be questioned for morphologies like folded mountain ranges or fields of parallel sand dunes. However, it must be remembered that in planetary applications the scales of roughness involved range from greater than a few soil particle diameters to just below the resolution of the observing instrument, that is, typically of the order of a millimeter to several kilometers. Because effects of material strength and soil cohesiveness are size dependent, the largest slopes, which dominate the reflectance, will occur at the small end of this size range. Departures from the horizontal induced by such erosive agents as microcratering, eolian gusting, and fluvial action are likely to be reasonably isotropic in azimuth on the dominating small scales, even though not necessarily on the less important larger scales.

No other assumptions about the geometry of the roughness are made. The present treatment attempts to keep the morphology as general as possible.

The general procedure of the derivation will be as follows. First, expressions which are mathematically rigorous will be derived and the parameters necessary for their evaluation defined. Since the effects are maximum at grazing illumination and viewing, these expressions will be evaluated exactly under these conditions. To obtain useful approximations the equations will also be evaluated for vertical viewing and illumination. The resulting expressions will be connected by analytic extrapolation to give a solution for intermediate angles.

IV. DERIVATION

The actual surface of the planet can be imagined to consist of an assemblage of smooth, unresolved facets of area A_f of a particulate material, where A_f is large compared with the cross-sectional areas of the particles but small compared with the area viewed by the detector. The normals to the facets are tilted at various angles θ with respect to the local vertical and in directions ζ relative to the azimuth of the source of illumination.

Let $a(\theta)$ be the function which describes the distribution of tilts. In general, it would be a function of both θ and ζ but, by assumption 4, a is independent of ζ. Let the slope distribution function be normalized so that

$$\int_0^{\pi/2} a(\theta)d\theta = 1, \tag{4}$$

and characterized by a mean slope angle $\bar{\theta}$ defined by

$$\tan\bar{\theta} = (2/\pi)\int_0^{\pi/2} \tan\theta a(\theta)\, d\theta. \tag{5}$$

Let the facets consist of a material which, if it covered a perfectly smooth planet, would reflect an amount of light

$$I(i,e,g) = Jr_S(i,e,g)\Delta\omega D^2 \quad (6)$$

when illuminated by collimated light of intensity J and observed from a distance D by a detector whose acceptance solid angle is $\Delta\omega$; that is, r_S is the bidirectional reflectance function of the surface material in macroscopically smooth form. Then the power emitted into unit solid angle per unit surface area would be

$$Y_S = Jr_S \cos e. \quad (7)$$

The amount of light reaching the detector from the area on the surface of the planet within $\Delta\omega$ with nominal values of i, e, and g actually comes from many facets tilted at a variety of angles and can be written

$$I(i,e,g) = J\int_{(i,v)} r_S(i_t,e_t,g)\cos e_t dA_t(\theta,\zeta), \quad (8)$$

where the subscript t on i, e, and A denotes values appropriate to an incremental surface of area $dA_t(\theta,\zeta) = A_t a(\theta)d\theta d\zeta$ tilted at angles (θ,ζ), and the symbol (i,v) indicates that the integration is to be taken only over those surface facets which are both illuminated and visible.

The light $I(i,e,g)$ reaching the detector is interpreted as if it came from a smooth, horizontal surface of area $A = D^2\Delta\omega \sec e$, where $A \gg A_t$ and D is the slant range, and having an effective bidirectional reflectance function $r_R(i,e,g)$; that is,

$$I(i,e,g) = AJr_R(i,e,g)\cos e = Jr_R\Delta\omega D^2. \quad (9)$$

The objective of this paper is to derive a correction to r_S to obtain r_R.

Macroscopic roughness has two important effects: one is that unresolved shadows are cast on one part of the surface by another part. The second is that, as the surface is viewed and illuminated at increasing angles, the facets which are tilted away from the observer or source tend to be hidden or in shadow, so that the surfaces which are visible and illuminated tend to be tilted preferentially toward the detector or source. To account for both of these effects I seek to write the bidirectional reflectance function r_R of the rough surface as the product of a shadowing function S and the bidirectional reflectance r_S of a smooth surface of area A' tilted at effective angles i' and e', but with the same phase angle g. That is, I wish to write the reflectance in the form

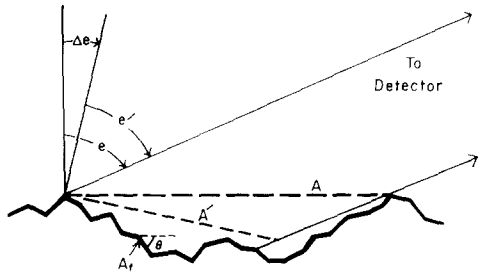

FIG. 1. Schematic diagram of the intersection of the surface and a vertical plane containing the detector. Shown are the actual surface consisting of a multitude of unresolved facets A_t, the nominal surface A, and the effective tilted surface A'. A cut by a vertical plane containing the source would be similar.

$$r_R(i,e,g) = r_S(i',e',g)S(i,e,g). \quad (10)$$

Then from (9) the intensity coming from A can be written as

$$I(i,e,g) = A'Jr_S(i',e',g)\cos e' S(i,e,g), \quad (11)$$

where A' and A are related by (see Fig. 1)

$$A'\cos e' = A\cos e. \quad (12)$$

Rewriting and combining Eqs. (8), (10), and (11) gives

$$AY_R(i,e,g) = A'Y_S(i',e',g)S(i,e,g) = \int_{(i,v)} Y_S(i_t,e_t,g)dA_t, \quad (13)$$

where

$$Y_R(i,e,g) = Jr_R(i,e,g)\cos e,$$

$$Y_S(i',e',g) = Jr_S(i',e',g)\cos e',$$

$$Y_S(i_t,e_t,g) = Jr_S(i_t,e_t,g)\cos e_t.$$

Let

$$\mu_0 = \cos i, \quad (14)$$

$$\mu = \cos e, \quad (15)$$

$$\mu_0' = \cos i', \tag{16}$$

$$\mu' = \cos e'. \tag{17}$$

The other angles are related by

$$\mu_{0t} = \cos i_t = \cos i \cos\theta + \sin i \sin\theta \cos\zeta, \tag{18}$$

$$\mu_t = \cos e_t = \cos e \cos\theta + \sin e \sin\theta \cos(\zeta - \Psi). \tag{19}$$

Note that g is the same for all surface facets within the viewed area.

To find μ_0', μ', and S expand the Y_S functions on both sides of the second equality in Eq. (13) in Taylor series about μ_0 and μ, and use (12) to obtain

$$\begin{aligned}
\frac{A\mu}{\mu'} S \Big[& Y_S(\mu_0,\mu,g) + \frac{\partial Y_S}{\partial \mu_0'}\Big|_{\mu_0,\mu} (\mu_0' - \mu_0) \\
& + \frac{\partial Y_S}{\partial \mu'}\Big|_{\mu_0,\mu} (\mu' - \mu) + \cdots \Big] = \int_{(i,v)} \\
& \Big[Y_S(\mu_0,\mu,g) + \frac{\partial Y_S}{\partial \mu_{0t}}\Big|_{\mu_0,\mu} (\mu_{0t} - \mu_0) \\
& + \frac{\partial Y_S}{\partial \mu_t}\Big|_{\mu_0,\mu} (\mu_t - \mu) + \cdots \Big] dA_t \\
= \; & Y_S(\mu_0,\mu,g) \int_{(i,v)} dA_t + \frac{\partial Y_S}{\partial \mu_0} \int_{(i,v)} \\
& (\mu_{0t} - \mu_0) dA_t + \frac{\partial Y_S}{\partial \mu} \int_{(i,v)} \\
& (\mu_t - \mu) dA_t + \cdots .
\end{aligned} \tag{20}$$

Since μ_0 and μ are independent variables and Y_S is an arbitrary function of μ_0 and μ, (20) will be satisfied if the coefficients of Y_S and its partial derivatives are separately equal on both sides of the equality. This gives

$$S = (\mu'/\mu A) \int_{(i,v)} dA_t, \tag{21}$$

$$\mu_0' = \int_{(i,v)} \mu_{0t} dA_t \Big/ \int_{(i,v)} dA_t, \tag{22}$$

and

$$\mu' = \int_{(i,v)} \mu_t dA_t \Big/ \int_{(i,v)} dA_t. \tag{23}$$

Similar expressions for higher powers of μ_0' and μ' can be found, but are not necessary because, in principle, once μ_0', μ' and S are found, they can be inserted back into (10) to give r_R. Thus, the problem of scattering from a rough surface is reduced to evaluating Eqs. (21)–(23). Note that this derivation does not assume that $\mu_0' - \mu_0$ and $\mu' - \mu$ are small, only that Y_S is mathematically well behaved so that expansion in a Taylor series at any point is possible.

In general, there will be two types of shadows. Some of the facets will not contribute to the surface brightness because they are tilted by an angle of more than $\pi/2$ to the direction to the source or detector; such facets will be said to be in a "tilt shadow." Some facets will not contribute because other parts of the surface block either the view of the detector or the light from the source; these facets will be said to lie in a "projected shadow." Following Saunders (1967) it is assumed that any facet not in a tilt shadow has the same statistical probability of lying in a projected shadow, independent of the slope or azimuth angle of its tilt.

Let p be the probability that a facet is not in a projected shadow. Then in Eq. (20) $Y_S(\mu_{0t},\mu_t,g)$ can be multiplied by p if at the same time the boundaries of the integration are replaced by the tilt shadow boundaries. This has the effect of multiplying both the numerators and denominators in (22) and (23) by p, which thus cancels in these equations. Therefore, writing out the expressions for μ_{0t}, μ_t, and dA_t explicitly, (22) and (23) become

$$\mu_0' = \frac{\cos i \int_{(\text{tilt})} \cos\theta a(\theta) d\theta d\zeta + \sin i \int_{(\text{tilt})} \sin\theta \cos\zeta a(\theta) d\theta d\zeta}{\int_{(\text{tilt})} a(\theta) d\theta d\zeta} \tag{24}$$

and

$$\mu' = \frac{\cos e \int_{(\text{tilt})} \cos\theta a(\theta) d\theta d\zeta + \sin e \int_{(\text{tilt})} \sin\theta \cos(\zeta - \Psi) a(\theta) d\theta d\zeta}{\int_{(\text{tilt})} a(\theta) d\theta d\zeta}, \tag{25}$$

where (tilt) denotes the boundary of the tilt shadow region.

Let A_T be the total rough area included within the nominal area A, whether visible and illuminated or not,

$$A_T = \int_{\text{all}(\theta,\zeta)} dA_t.$$

Also, A is just the projection of all facets onto the horizontal plane

$$A = \int_{\text{all}(\theta,\zeta)} \cos\theta dA_t.$$

Because of azimuthal symmetry

$$A/A_T = \int_0^{\pi/2} \cos\theta a(\theta)d\theta \Big/ \int_0^{\pi/2} a(\theta)d\theta \equiv \langle\cos\theta\rangle.$$

Thus, expression (21) for S can be written

$$S(\mu_0,\mu,\Psi) = (\mu'/\mu)(A_T/A)\left(\int_{(i,v)} dA_t/A_T\right) = (\mu'/\mu\langle\cos\theta\rangle)F_{i,v}, \tag{26}$$

where

$$F_{iv}(\mu_0,\mu,\Psi) = \int_{(i,v)} dA_t/A_T$$

is the probability that a facet will be both illuminated and visible.

1. The Case When $i \leq e$

It is convenient to consider separately the situations when $i \leq e$ and $i \geq e$. Define the quantities $F_i(i)$ and $F_e(e)$, respectively, as the fraction of the facets which are illuminated and the fraction which are visible. Because of azimuthal symmetry F_i and F_e are independent of Ψ. Let f be the fraction of the illumination shadow which overlaps the visibility shadow.

When $i \leq e$ the illumination shadow is always smaller than the visibility shadow and may be regarded as partially hidden by it. When $\Psi = 0$ and $i < e$, the illumination shadow is completely hidden, so that $F_{iv}(\mu_0,\mu,0) = F_e$. But when $\Psi = 0$, no shadows are visible and the detector's field of view is completely filled by surfaces which are visible and totally illuminated. Thus,

$$S(\mu_0,\mu,0) = (\mu'^0/\mu\langle\cos\theta\rangle)F_e = 1,$$

where

$$\mu'^0 = \mu'(\Psi = 0). \tag{27}$$

Hence,

$$F_e(e) = \mu\langle\cos\theta\rangle/\mu'^0. \tag{28}$$

Because of the assumption of azimuthal symmetry of the surface morphology, $F_e(e)$ must be independent of Ψ, and also $F_i(i)$ must have the same functional dependence on i as $F_e(e)$ does on e; thus,

$$F_i(i) = \mu_0\langle\cos\theta\rangle/\mu_0'^0, \tag{29}$$

where

$$\mu_0'^0 = \mu_0'(\Psi = 0). \tag{30}$$

Let the quantities A_e and A_i be defined by

$$A_e/A_T = 1 - F_e,$$

where A_e/A_T is the fraction of the facets in the visibility shadows, and

$$A_i/A_T = 1 - F_i$$

is the fraction of the facets in the illumination shadows. These include both the tilt and projected shadows. When $\Psi = 0$, all of the illumination shadows are hidden in the visibility shadows; the visibility and illumination shadows are perfectly correlated, so that

$$f = 1$$

and

$$F_{iv} = F_e = 1 - A_e/A_T.$$

As Ψ increases, a fraction $1 - f$ of the illumination shadows will be exposed. When $\Psi = \pi$, $f = 0$, and the two types of shadows are completely uncorrelated, so that

$$\begin{aligned} F_{iv} &= 1 - A_e/A_T - A_i/A_T + (A_e/A_T)(A_i/A_T) \\ &= (1 - A_e/A_T)(1 - A_i/A_T) \\ &= F_eF_i, \end{aligned}$$

where the term $A_e A_i / A_T^2$ corrects for the amount of random overlap. The last equation states that when the two shadows are completely uncorrelated the probability that a facet will be both illuminated and visible is the product of the separate probabilities.

When $\Psi < \pi$, A_i in the last expression for F_{iv} must be replaced by $(1 - f)A_i/(A_T - fA_i)$, where this term accounts for the facts that only a portion $1 - f$ of the illumination shadow is randomly exposed, and only an area $A_T - fA_i$ is available to be occupied by this uncorrelated part of the illumination shadow. Thus, the general expression for the probability that a facet will be both illuminated and visible is

$$\begin{aligned} F_{iv} &= [1 - A_e/A_T] \\ &\qquad [1 - (1 - f)A_i/(A_T - fA_i)] \\ &= [1 - A_e/A_T][1 - A_i/A_T]/[1 - fA_i/A_T] \\ &= F_e F_i/(1 - f + fF_i). \end{aligned}$$

Combining this result with with (26), (28), and (29) gives

$$\begin{aligned} S(i,e,\Psi) = (\mu'/\mu'^0)(\mu_0/\mu_0'^0)\langle\cos\theta\rangle \\ [1 - f + f(\mu_0/\mu_0'^0)\langle\cos\theta\rangle]^{-1}. \end{aligned} \quad (31)$$

Thus far, the derivation has been rigorous. In the remainder of this subsection approximate, analytic expressions for μ_0', μ', and S which are suitable for practical calculations will be developed. This will be done by evaluating equations (24) and (25) exactly for i and e near $\pi/2$ and near 0; the solutions thus obtained will be connected by analytic extrapolation to furnish expressions for intermediate angles.

First a suitable expression for f, the fraction of the illumination shadow hidden in the visibility shadow, will be found. It will be assumed that f is a function of Ψ only and is independent of i and e, which will be a good approximation at grazing illumination and viewing. The surface can be considered as being made up of protuberances and depressions of mean width d and mean height $\tan\theta d/2$. As Ψ increases from zero the fraction of the tilt illumination shadows exposed will increase approximately linearly with Ψ and be completely exposed at $\Psi = \pi$; hence this component of f will decrease approximately as Ψ/π. However, for e and i near $\pi/2$ the projected shadows are cast by objects of width $\sim d$ onto surfaces a distance $\sim d$ away, so that these shadows are nearly completely exposed when $\Psi > 1$ radian. Since for large angles the shadow consists roughly equally of tilt and projected components the fraction exposed at $\Psi = 1$ is approximately $(\frac{1}{2}) \times (1/\pi) + (\frac{1}{2}) \times 1 \approx \frac{2}{3}$. Thus the fraction hidden may be approximated by a function which decreases rapidly from a value of 1 at $\Psi = 0$, to a value of about $1 - \frac{2}{3} = \frac{1}{3}$ at $\Psi = 1$ and then approaches 0 as Ψ approaches π. A simple function with the required properties is

$$f(\Psi) = \exp[-2\tan(\Psi/2)]. \quad (32)$$

Returning to μ_0' and μ', only the tilt shadows affect these quantities. The boundary of the tilt illumination shadow is given by (18) with $i_t = \pi/2$, or

$$\cos\zeta = -\cot\theta\cot i. \quad (33)$$

This equation has no solution when $0 \le \theta < \pi/2 - i$, but ζ lies between $\pi/2$ and $3\pi/2$ when $\pi/2 - i \le \theta \le \pi/2$. Similarly, the boundary of the tilt visibility shadow is given by (19) with $e_t = \pi/2$:

$$\cos(\zeta - \Psi) = -\cot\theta\cot e, \quad (34)$$

which has no solution when $0 \le \theta < \pi/2 - e$, but ζ lies between $\pi/2 + \Psi$ and $3\pi/2 + \Psi$ when $\pi/2 - e \le \theta \le \pi/2$.

Equations (24) and (25) are readily evaluated at $i = e = 0$ and $\pi/2$. For vertical illumination and viewing the integrals over $\cos\zeta$ and $\cos(\zeta - \Psi)$ vanish, and

$$i = e = 0: \qquad \mu_0' = \mu' = \langle\cos\theta\rangle. \quad (35)$$

If the tilt shadows are represented in a polar diagram with θ and ζ, respectively, as the radial and angular variables, then when $i = e = \pi/2$ the tilt shadow boundaries are the straight radial lines $\zeta = \Psi - \pi/2$ and $\zeta = \pi/2$, while the limits on θ are 0 to $\pi/2$. Hence,

$i = e = \pi/2$:

$$\mu_0' = \mu' = (1 + \cos \Psi)\langle \sin \theta \rangle / (\pi - \Psi), \tag{36}$$

where

$$\langle \sin \theta \rangle = \int_0^{\pi/2} \sin \theta a(\theta)\, d\theta.$$

When $\Psi = 0$ Eq. (36) shows that the effective surface is tilted toward the source and detector by an amount $\sin^{-1}(2\langle \sin \theta \rangle / \pi)$.

For intermediate values of i and e the integrals are much more complicated because the shadow boundaries (33) and (34) are overlapping curves in the $\theta - \zeta$ diagram. However, these integrals could be evaluated at any i, e, and Ψ if the curved shadow boundaries could be approximated in the diagram by appropriate segments of straight radial lines of constant ζ and circles of constant θ. This approach is carried out as follows.

The effect of the illumination shadow alone on μ_0' may be ascertained by setting $e = 0$ and using (33) as the (tilt) boundary in (24). The integration over ζ in the three integrals in the numerator and denominator of (24) may then be carried out exactly to give, respectively,

$$\int_{(\text{tilt})} \cos \theta a(\theta) d\theta d\zeta = \int_0^{\pi/2 - i} 2\pi \cos \theta a(\theta) d\theta + \int_{\pi/2 - i}^{\pi/2} 2 \sin^{-1}(1 - \cot^2\theta \cot^2 i)^{1/2} \cos \theta a(\theta) d\theta, \tag{37a}$$

$$\int_{(\text{tilt})} \sin \theta \cos \zeta a(\theta) d\theta d\zeta = \int_{\pi/2 - i}^{\pi/2} (1 - \cot^2\theta \cot^2 i)^{1/2} \sin \theta a(\theta) d\theta, \tag{37b}$$

$$\int_{(\text{tilt})} a(\theta) d\theta d\zeta = \int_0^{\pi/2 - i} a(\theta) d\theta + \int_{\pi/2 - i}^{\pi/2} \sin^{-1}(1 - \cot^2\theta \cot^2 i)^{1/2} a(\theta) d\theta, \tag{37c}$$

where the value of the $\sin^{-1}$ is to be taken between $\pi/2$ and π. Now, the factor $(1 - \cot^2\theta \cot^2 i)^{1/2}$ has the following properties: it rises with infinite slope from the value zero at $\theta = \pi/2 - i$ to the value unity at $\theta = \pi/2$, where it has a slope of zero. Thus, as a beginning approximation this factor may be replaced by a unit step function at $\theta = \pi/2 - i$. (This approximation will be corrected for below.) Then (37) becomes

$$\int_{(\text{tilt})} \cos \theta a(\theta) d\theta d\zeta \simeq \int_0^{\pi/2 - i} 2\pi \cos \theta a(\theta) d\theta + \int_{\pi/2 - i}^{\pi/2} \pi \cos \theta a(\theta) d\theta, \tag{38a}$$

$$\int_{(\text{tilt})} \sin \theta \cos \zeta a(\theta) d\theta d\zeta \simeq \int_{\pi/2 - i}^{\pi/2} 2 \sin \theta a(\theta) d\theta, \tag{38b}$$

$$\int_{(\text{tilt})} a(\theta) d\theta d\zeta \simeq \int_0^{\pi/2 - i} 2\pi a(\theta) d\theta + \int_{\pi/2 - i}^{\pi/2} \pi a(\theta) d\theta. \tag{38c}$$

Similarly, the effect of the visibility shadow alone on μ_0' may be ascertained by setting $i = 0$ and using (34) in (24) to obtain

$$\int_{(\text{tilt})} \cos \theta a(\theta) d\theta d\zeta = \int_0^{\pi/2 - e} \cos \theta a(\theta) d\theta + \int_{\pi/2 - e}^{\pi/2} 2 \sin^{-1}(1 - \cot^2\theta \cot^2 e)^{1/2} \cos \theta a(\theta) d\theta, \tag{39a}$$

$$\int_{(\text{tilt})} \sin \theta \cos \zeta a(\theta) d\theta d\zeta = \int_{\pi/2 - e}^{\pi/2} 2 \cos \Psi (1 - \cot^2\theta \cot^2 e)^{1/2} \sin \theta a(\theta) d\theta, \tag{39b}$$

$$\int_{(\text{tilt})} a(\theta) d\theta d\zeta = \int_0^{\pi/2 - e} 2\pi a(\theta) d\theta + \int_{\pi/2 - e}^{\pi/2} 2 \sin^{-1}(1 - \cot^2\theta \cot^2 e)^{1/2} a(\theta) d\theta, \tag{39c}$$

which, upon approximating $(1 - \cot^2\theta \cot^2 e)^{1/2}$ by a unit step function at $\theta = \pi/2 - e$, becomes

$$\int_{(\text{tilt})} \cos\theta a(\theta) d\theta d\zeta \simeq \int_0^{\pi/2-e} 2\pi \cos\theta a(\theta) d\theta + \int_{\pi/2-e}^{\pi/2} \pi \cos\theta a(\theta) d\theta, \quad (40a)$$

$$\int_{(\text{tilt})} \sin\theta \cos\zeta a(\theta) d\theta d\zeta \simeq \int_{\pi/2-e}^{\pi/2} 2 \cos\Psi \sin\theta a(\theta) d\theta, \quad (40b)$$

$$\int_{(\text{tilt})} a(\theta) d\theta d\zeta \simeq \int_0^{\pi/2-e} 2\pi a(\theta) d\theta + \int_{\pi/2-e}^{\pi/2} \pi a(\theta) d\theta. \quad (40c)$$

These approximations are equivalent to replacing the curved illumination shadow boundary in the $\theta - \zeta$ diagram by a square-cornered shadow bounded by the radial lines $\zeta = \pi/2$ and $3\pi/2$ and the circles $\theta = \pi/2 - i$ and $\pi/2$, and replacing the visibility shadow by a square-cornered shadow bounded by the radial lines $\zeta = \pi/2 + \Psi$ and $3\pi/2 + \Psi$ and the circles $\theta = \pi/2 - e$ and $\pi/2$. These squared shadows are illustrated in Fig. 2. At grazing illumination and viewing these approximations become exact. With the simplified boundaries of the squared-shadow approximation the three integrals in Eq. (24) may be evaluated for the case when neither i, e, nor Ψ are zero to give

$$\int_{(\text{tilt})} \cos\theta a(\theta) d\theta d\zeta \simeq \int_0^{\pi/2-e} 2\pi \cos\theta a(\theta) d\theta + \int_{\pi/2-e}^{\pi/2} \pi \cos\theta a(\theta) d\theta - \frac{\Psi}{\pi} \int_{\pi/2-i}^{\pi/2} \pi \cos\theta a(\theta) d\theta, \quad (41a)$$

$$\int_{(\text{tilt})} \sin\theta \cos\zeta a(\theta) d\theta d\zeta \simeq \int_{\pi/2-e}^{\pi/2} 2 \cos\Psi \sin\theta a(\theta) d\theta + \int_{\pi/2-i}^{\pi/2} (1 - \cos\Psi) \sin\theta a(\theta) d\theta, \quad (41b)$$

$$\int_{(\text{tilt})} a(\theta) d\theta d\zeta \simeq \int_0^{\pi/2-e} 2\pi a(\theta) d\theta + \int_{\pi/2-e}^{\pi/2} \pi a(\theta) d\theta - \frac{\Psi}{\pi} \int_{\pi/2-i}^{\pi/2} \pi a(\theta) d\theta. \quad (41c)$$

The first term in (41b) is the same as (40b). The second term corrects for the fraction of the illumination shadow visible and is identical with (38b), weighted by the integral of $\cos\zeta d\zeta$ over the portion of the $\theta - \zeta$ diagram not covered by tilt shadows. The first two terms in (41a) are the same as (40a). The last term corrects for the fraction of the illumination shadow sticking out from behind the visibility shadow, and is identical with the last term in (38a) weighted by the integral of $d\zeta$. Equation (41c) is similarly related to (40c) and (38c).

The approximation may be improved by replacing the integrals in (41), which appear in (38) and (40) and result from the squared-shadow boundaries, by their more exact counterparts in (37) and (39), respectively, which describe the curved shadows. This gives

$$\int_{(\text{tilt})} \cos\theta a(\theta) d\theta d\zeta \simeq \int_0^{\pi/2-e} 2\pi \cos\theta a(\theta) d\theta + \int_{\pi/2-e}^{\pi/2} 2 \sin^{-1}(1 - \cot^2\theta \cot^2 e)^{1/2} \cos\theta a(\theta) d\theta - \frac{\Psi}{\pi} \int_{\pi/2-i}^{\pi/2} 2 \sin^{-1}(1 - \cot^2\theta \cot^2 i)^{1/2} \cos\theta a(\theta) d\theta, \quad (42a)$$

$$\int_{(\text{tilt})} \sin\theta \cos\zeta a(\theta)d\theta d\zeta \simeq \int_{\pi/2-e}^{\pi/2} 2\cos\Psi(1-\cot^2\theta\cot^2 e)^{1/2}\sin\theta a(\theta)d\theta + \int_{\pi/2-i}^{\pi/2}(1-\cos\Psi)(1-\cot^2\theta\cot^2 i)^{1/2}\sin\theta a(\theta)d\theta, \quad (42b)$$

$$\int_{(\text{tilt})} a(\theta)d\theta d\zeta \simeq \int_0^{\pi/2-e} 2\pi a(\theta)d\theta + \int_{\pi/2-e}^{\pi/2} 2\sin^{-1}(1-\cot^2\theta\cot^2 e)^{1/2}a(\theta)d\theta - \frac{\Psi}{\pi}\int_{\pi/2-i}^{\pi/2} 2\sin^{-1}(1-\cot^2\theta\cot^2 i)^{1/2}a(\theta)d\theta, \quad (42c)$$

where the value of $\sin^{-1}(1-\cot^2\theta\cot^2 e)^{1/2}$ is to be taken between $\pi/2$ and π, but the value of $\sin^{-1}(1-\cot^2\theta\cot^2 i)^{1/2}$ must be taken between 0 and $\pi/2$.

Equation (42) is evaluated analytically as follows. Define the average value of any function $F(\theta)$ as $\langle F(\theta)\rangle = \int_0^{\pi/2} F(\theta)a(\theta)d\theta$. When i and e are close to $\pi/2$ the integrals in (42) may be expanded in Taylor series in cot e and cot i to give

$$\begin{aligned}\int_{(\text{tilt})} \cos\theta\, a(\theta)d\theta d\zeta &\simeq \pi\langle\cos\theta\rangle + 2\langle\cot\theta\cos\theta\rangle\cot e - \frac{\Psi}{\pi}(\pi\langle\cos\theta\rangle - 2\langle\cot\theta\cos\theta\rangle\cot i)\\ &= \pi\langle\cos\theta\rangle\left[2-\left(1-\frac{2}{\pi}\frac{\langle\cot\theta\cos\theta\rangle}{\langle\cos\theta\rangle}\cot e\right)-\frac{\Psi}{\pi}\left(1-\frac{2}{\pi}\frac{\langle\cot\theta\cos\theta\rangle}{\langle\cos\theta\rangle}\cot i\right)\right]\\ &\simeq \pi\langle\cos\theta\rangle\left[2-\exp\left(-\frac{2}{\pi}\frac{\langle\cot\theta\cos\theta\rangle}{\langle\cos\theta\rangle}\cot e\right)\right.\\ &\qquad\left.-\frac{\Psi}{\pi}\exp\left(-\frac{2}{\pi}\frac{\langle\cot\theta\cos\theta\rangle}{\langle\cos\theta\rangle}\cot i\right)\right], \quad (43a)\end{aligned}$$

$$\begin{aligned}\int_{(\text{tilt})} \sin\theta\cos\zeta a(\theta)d\theta d\zeta &\simeq 2\cos\Psi\left[\langle\sin\theta\rangle-\frac{1}{2}\langle\cot^2\theta\sin\theta\rangle\cot^2 e\right]\\ &\quad+(1-\cos\Psi)\left[\langle\sin\theta\rangle-\frac{1}{2}\langle\cot^2\theta\sin\theta\rangle\cot^2 i\right]\\ &= 2\langle\sin\theta\rangle\left[\cos\Psi\left(1-\frac{1}{2}\frac{\langle\cot\theta\cos\theta\rangle}{\langle\sin\theta\rangle}\cot^2 e\right)\right.\\ &\qquad\left.+\sin^2\frac{\Psi}{2}\left(1-\frac{1}{2}\frac{\langle\cot\theta\cos\theta\rangle}{\langle\sin\theta\rangle}\cot^2 i\right)\right]\\ &\simeq 2\langle\sin\theta\rangle\left[\cos\Psi\exp\left(-\frac{\langle\cot\theta\cos\theta\rangle}{2\langle\sin\theta\rangle}\cot^2 e\right)\right.\\ &\qquad\left.+\sin^2\frac{\Psi}{2}\exp\left(-\frac{\langle\cot\theta\cos\theta\rangle}{2\langle\sin\theta\rangle}\cot^2 i\right)\right], \quad (43b)\end{aligned}$$

$$\begin{aligned}\int_{(\text{tilt})} a(\theta)d\theta d\zeta &\simeq \pi + 2\langle\cot\theta\rangle\cot e - \frac{\Psi}{\pi}(\pi - 2\langle\cot\theta\rangle\cot i)\\ &= \pi\left[2-\left(1-\frac{2}{\pi}\langle\cot\theta\rangle\cot e\right)-\frac{\Psi}{\pi}\left(1-\frac{2}{\pi}\langle\cot\theta\rangle\cot i\right)\right]\\ &\simeq \pi\left[2-\exp\left(-\frac{2}{\pi}\langle\cot\theta\rangle\cot e\right)-\frac{\Psi}{\pi}\exp\left(-\frac{2}{\pi}\langle\cot\theta\rangle\cot i\right)\right]. \quad (43c)\end{aligned}$$

In order to proceed further it is necessary to choose a slope distribution function $a(\theta)$. Since (43) contains only averages of trigonometric functions weighted by $a(\theta)$ the equations are insensitive to the exact form of $a(\theta)$ used. Two distribution functions, Gaussian and exponential, which have been widely used in planetary applications (Saunders, 1967; Hagfors, 1968) were investigated. The numerical differences be-

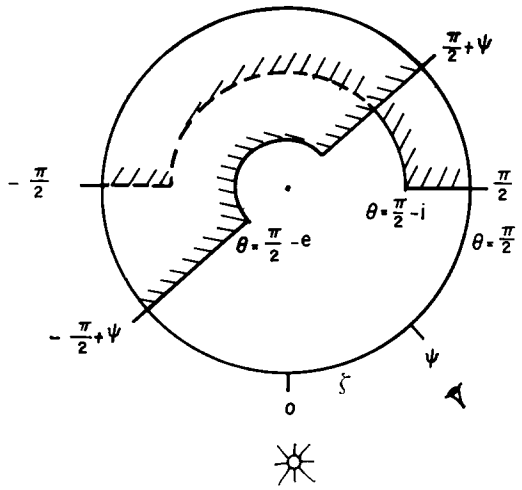

FIG. 2. Schematic diagram showing the square-cornered approximation to the tilt shadows in (θ, ζ) space for the case when $i \leq e$. The projected shadows are assumed to be randomly distributed over the part of (θ,ζ) space not in tilt shadows. See text for definitions of the terms "tilt" and "projected" shadows.

tween the two turned out to be quite minor; hence, the Gaussian was chosen.

Let $a_1(\theta)d\theta$ be the function describing the distribution of slopes on any vertical cut with arbitrary azimuth through the surface. Then $a_1(\theta)$ is assumed to be of the form

$$a_1(\theta)d\theta = A \exp[-\tan^2\theta/B \tan^2\bar{\theta}]d(\tan\theta),$$

where A and B are constants. In general, if $a_1(\theta)d\theta$ is the one-dimensional distribution, then the corresponding two-dimensional, azimuth-independent slope distribution function is

$$a_1(\theta) \sin\theta d\theta d\zeta$$

(Hagfors, 1968). Thus $a(\theta)$ is taken as

$$a(\theta) = A \exp[-\tan^2\theta/ B \tan^2\bar{\theta}]\sec^2\theta \sin\theta. \quad (44)$$

Assumption (2), that the mean slope $\bar{\theta}$ is not too large, will now be used for the first time. Using the slope distribution function (44) and applying (4) and (5) it is found that, to second order in $\bar{\theta}$,

$$A = 2/\pi \tan^2\bar{\theta},$$

$$B = \pi,$$

$$\langle\cot\theta\rangle = \cot\bar{\theta},$$

$$\langle\sin\theta\rangle = (\pi/2)\langle\cos\theta\rangle \tan\bar{\theta},$$

$$\langle\cot\theta\cos\theta\rangle = \cot\bar{\theta}\langle\cos\theta\rangle = (2/\pi)\cot^2\bar{\theta}\langle\sin\theta\rangle,$$

and

$$\langle\cos\theta\rangle = (1 + \pi\tan^2\bar{\theta})^{-1/2}. \quad (45)$$

Inserting these results into (43) and the resulting expressions into (24) gives

$$\mu_0' = \frac{1}{\sqrt{1+\pi\tan^2\bar{\theta}}}\left[\cos i + \sin i \tan\bar{\theta}\,\frac{\cos\Psi \exp\left(-\frac{\cot^2\bar{\theta}\cot^2 e}{\pi}\right) + \sin^2\frac{\Psi}{2}\exp\left(-\frac{\cot^2\bar{\theta}\cot^2 i}{\pi}\right)}{2 - \exp\left(-\frac{2}{\pi}\cot\bar{\theta}\cot e\right) - \frac{\Psi}{\pi}\exp\left(-\frac{2}{\pi}\cot\bar{\theta}\cot i\right)}\right]. \quad (46)$$

This expression is in the desired form and is exact for conditions of grazing and normal illumination and viewing.

Identical arguments give:

$$\mu' = \frac{1}{\sqrt{1+\pi\tan^2\bar{\theta}}}\left[\cos e + \sin e \tan\bar{\theta}\,\frac{\exp\left(-\frac{\cot^2\bar{\theta}\cot^2 e}{\pi}\right) - \sin^2\frac{\Psi}{2}\exp\left(-\frac{\cot^2\bar{\theta}\cot^2 i}{\pi}\right)}{2 - \exp\left(-\frac{2}{\pi}\cot\bar{\theta}\cot e\right) - \frac{\Psi}{\pi}\exp\left(-\frac{2}{\pi}\cot\bar{\theta}\cot i\right)}\right]. \quad (47)$$

If desired, roughness expressions correct to higher order in $\bar{\theta}$ may be found using (24), (25), (43), and (44), but probably would not be justified because of assumption (3).

Equations (46) and (47) describe the effective tilt of the surface. Although they appear complicated, their behavior is relatively simple. When i and e are smaller than about $\pi/2 - \bar{\theta}$, $\mu_0' \approx \mu_0\langle\cos\theta\rangle$ and $\mu' \approx \mu\langle\cos\theta\rangle$. However, when i or e are larger than about $\pi/2 - \bar{\theta}$, the effective surface is tilted toward the source and detector by $\sim\bar{\theta}$. The effective tilt approaches zero as Ψ approaches π.

Finally, the factors $\mu_0'^0$ and μ'^0 in S can be evaluated

$$\mu_0'^0 = \frac{1}{\sqrt{1 + \pi\tan^2\bar{\theta}}}\left[\cos i + \sin i \tan\bar{\theta}\frac{\exp\left(-\frac{\cot^2\bar{\theta}\cot^2 i}{\pi}\right)}{2 - \exp\left(-\frac{2}{\pi}\cot\bar{\theta}\cot i\right)}\right], \tag{48}$$

and

$$\mu'^0 = \frac{1}{\sqrt{1 + \pi\tan^2\bar{\theta}}}\left[\cos e + \sin e \tan\bar{\theta}\frac{\exp\left(-\frac{\cot^2\bar{\theta}\cot^2 e}{\pi}\right)}{2 - \exp\left(-\frac{2}{\pi}\cot\bar{\theta}\cot e\right)}\right]. \tag{49}$$

Then from (31),

$$S = (\mu'/\mu'^0)(\mu_0/\mu_0'^0)\frac{1}{\sqrt{1 + \pi\tan^2\bar{\theta}}}\left[1 - f + \frac{f}{\sqrt{1 + \pi\tan^2\bar{\theta}}}(\mu_0/\mu_0'^0)\right]^{-1}.$$

2. The Case When $i \geq e$

Similar reasoning for the situation when $i > e$ leads to the following expressions:

$$\mu_0' = \frac{1}{\sqrt{1 + \pi\tan^2\bar{\theta}}}\left[\cos i + \sin i\tan\bar{\theta}\frac{\exp\left(-\frac{\cot^2\bar{\theta}\cot^2 i}{\pi}\right) - \sin^2\frac{\Psi}{2}\exp\left(-\frac{\cot^2\bar{\theta}\cot^2 e}{\pi}\right)}{2 - \exp\left(-\frac{2}{\pi}\cot\bar{\theta}\cot i\right) - \frac{\Psi}{\pi}\exp\left(-\frac{2}{\pi}\cot\bar{\theta}\cot e\right)}\right] \tag{50}$$

$$\mu' = \frac{1}{\sqrt{1 + \pi\tan^2\bar{\theta}}}\left[\cos e + \sin e\tan\bar{\theta}\frac{\cos\Psi\exp\left(-\frac{\cot^2\bar{\theta}\cot^2 i}{\pi}\right) + \sin^2\frac{\Psi}{2}\exp\left(-\frac{\cot^2\bar{\theta}\cot^2 e}{\pi}\right)}{2 - \exp\left(-\frac{2}{\pi}\cot\bar{\theta}\cot i\right) - \frac{\Psi}{\pi}\exp\left(-\frac{2}{\pi}\cot\bar{\theta}\cot e\right)}\right] \tag{51}$$

$$S(i, e, \Psi) = (\mu'/\mu'^0)(\mu_0/\mu_0'^0)\frac{1}{\sqrt{1 + \pi\tan^2\bar{\theta}}}\left[1 - f + \frac{f}{\sqrt{1 + \pi\tan^2\bar{\theta}}}(\mu/\mu'^0)\right]^{-1} \tag{52}$$

where $f(\Psi)$, $\mu_0'^0$, and μ'^0 are the same as for the $i \leq e$ case and are given, respectively, by (32), (48), and (49), except that $f(\Psi)$ is now to be interpreted as the fraction of the visibility shadow hidden in the illumination shadow.

V. APPLICATIONS TO DIFFERENTIAL PLANETARY PHOTOMETRY

The equations derived in the preceding section can be used to correct any arbitrary bidirectional reflectance of a smooth surface for effects of macroscopic roughness. In the first paper in this series (Hapke, 1981) a comprehensive photometric function for a smooth particulate surface was derived from the equation of radiative transfer. The reflectance includes effects of non-isotropic scattering, multiple-scattering, porosity, and blocking and shadowing by individual particles on a microscopic scale. The function is

$$r_S(i,e,g) = [\mu_0/(\mu_0 + \mu)]\,\frac{w}{4\pi}$$
$$\{[1 + B(g)]P(g) - 1 + H(\mu_0)H(\mu)\}, \quad (53)$$

where $B(g)$ is the backscatter function describing the opposition effect

$$B(g,h) = B_0\{1 - (\tan|g|/2h)$$
$$[3 - \exp(-h\cot|g|)]$$
$$[1 - \exp(h\cot|g|)]\}, \quad (54)$$

when $|g| \leq \pi/2$, and $B(g) = 0$ when $|g| > \pi/2$, B_0 is a semiempirical factor approximated by

$$B_0 \approx \exp(-w^2/2); \quad (55)$$

$$H(x) = (1 + 2x)/[1 + 2x(1 - w)^{1/2}]; \quad (56)$$

w is the average single-scattering albedo; $P(g)$ is the average single-particle scattering function normalized so that

$$(1/4\pi)\int_0^{\pi} P(g)\sin g\,dg = 1;$$

and h is a backscatter parameter related to the porosity of the soil. The parameter h is discussed in detail in Hapke (1963, 1981); it is essentially equal to the ratio of the mean size of the openings between soil particles to the extinction mean free path. It is double-valued and approaches zero as the porosity approaches either zero or one, with a maximum for intermediate porosities. Typical values are $h \sim 0.2$–0.6.

Inserting Eq. (53) into the results of Section IV gives the following photometric function for a rough-surfaced planetary regolith for the case when $g \geq 0$. The function when $g < 0$ can be obtained from the $g \geq 0$ function by simultaneously changing the signs of Λ and g.

1. When $i \leq e$ (or $\Lambda \leq -g/2$)

$$r_R(i,e,g) = \frac{w}{4\pi}\frac{\mu_0'}{\mu_0' + \mu'}\{[1 + B(g)]P(g) - 1 + H(\mu_0')H(\mu')\}$$
$$\frac{\mu'\mu_0}{\mu'^0\mu_0'^0\sqrt{1 + \pi\tan^2\bar{\theta}}\,[1 - f + f(\mu_0/\mu_0'^0\sqrt{1 + \pi\tan^2\bar{\theta}})]} \quad (57)$$

where $\bar{\theta}$ is the mean slope angle, defined by (5), and μ_0', μ', $\mu_0'^0$, μ'^0 and f are defined, respectively, by (46)–(49) and (32).

2. When $i \geq e$ (or $\Lambda \geq -g/2$)

$$r_R(i,e,g) = \frac{w}{4\pi}\frac{\mu_0'}{\mu_0' + \mu'}\{[1 + B(g)]P(g) - 1 + H(\mu_0')H(\mu')\}$$
$$\frac{\mu'\mu_0}{\mu'^0\mu_0'^0\sqrt{1 + \pi\tan^2\bar{\theta}}\,[1 - f + f(\mu/\mu'^0\sqrt{1 + \pi\tan^2\bar{\theta}})]} \quad (58)$$

where $\bar{\theta}$, μ_0', μ', $\mu_0'^0$, μ'^0, and f are defined, respectively, by (5), (50), (51), (48), (49), and (32).

3. Reciprocity

Equations (57) and (58) satisfy the Helmholtz reciprocity conditions

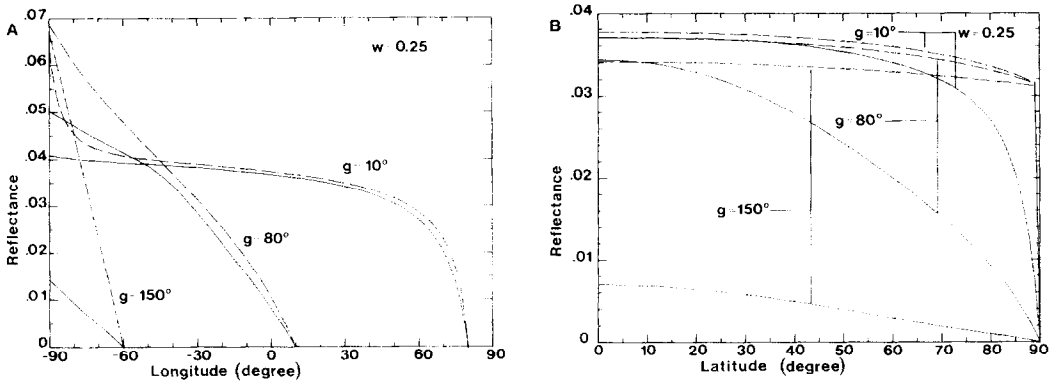

FIG. 3. Effects of macroscopic roughness on the brightness profiles of a low albedo ($w = 0.25$) planet at three phase angles g. For clarity the surface is assumed to be covered with isotropically scattering particles and the opposition effect is neglected. Solid lines, reflectance πr_R relative to a Lambert surface for $\bar{\theta} = 25°$; dashed lines, $\bar{\theta} = 0°$. (A) Profiles along the luminance equator. (B) Profiles along the central meridian of the illuminated part of the disk.

$$r_R(i,e,g)/\cos i = r_R(e,i,g)/\cos e.$$

Interchanging i and e in (57) divided by cos i gives the brightness of the reciprocal point (58) divided by cos e.

4. *Examples*

To illustrate the effects of roughness, Eqs. (57) and (58) were used to calculate reflectance profiles πr_R (A,L,g), relative to a Lambert surface, on a low albedo (w = 0.25) and a high albedo (w = 0.95) planet for $\bar{\theta} = 25°$. The results are shown in Figs. 3 and 4, along with smooth-surface brightness profiles for comparison. For simplicity these figures were calculated assuming isotropic scatterers ($P(g) = 1$) and no opposition effect ($h = 0$).

Figures 3A and 4A show reflectance versus longitude along the equator for several phase angles. Note that the bright limb surge, which is predicted by rigorous solutions to the radiative transfer equation to occur on low albedo planets, is removed by

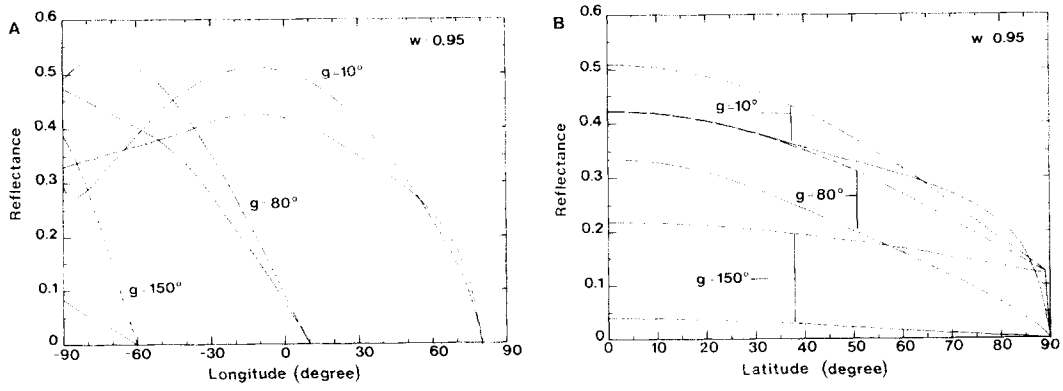

FIG. 4. Effects of macroscopic roughness on the brightness profiles of a high albedo (w = 0.95) planet at three phase angles g. For clarity the surface is assumed to be covered with isotropically scattering particles and the opposition effect is neglected. Solid lines, reflectance πr_R relative to a Lambert surface for $\bar{\theta} = 25°$; dashed lines, $\bar{\theta} = 0°$. (A) Profiles along the luminance equator. (B) Profiles along the central meridian of the illuminated part of the disk.

the roughness correction. Note also that at small phase angles the roughness may have opposite effects on limb and terminator brightness, depending on the albedo. The brightnesses are reduced if the albedo is low, but are increased if the albedo is high and multiple scattering is important. This behavior occurs because near the limb or terminator only areas tilted preferentially toward the observer or source, respectively, contribute to the brightness, and the reflectance is similar to that of a smooth surface closer to the center of the crescent, but suitably modified by S. These effects are not predicted by photometric functions which do not take effective tilt into account.

Figures 3B and 4B give the brightness versus latitude along the central meridian of the illuminated crescent. The effect of roughness is to cause the brightness to generally decrease with latitude. This result is in contrast to calculations made on the basis of rigorous solutions of the radiative transfer equation for smooth, low albedo planets, which predict that the reflectance is proportional to $\mu_0/(\mu_0 + \mu)$, and thus is independent of latitude (Eqs. (1) and (2)). However, in the rough-surface, low albedo case the manner in which the brightness decreases with latitude depends on the phase angle. At small phase angles the brightness is nearly independent of latitude, as observed for the Moon by Minnaert (1961). As g increases the polar darkening becomes more pronounced.

The theory is compared with observations of a real planet in Figs. 5A and B, which shows brightness profiles on the surface of Mercury, as observed by Mariner 10. The fit is seen to be quite good for a mean slope angle of 20°.

VI. INTEGRAL PLANETARY PHOTOMETRY

The integral brightness of a uniform spherical planet of radius R at phase angle g is found by integrating the intensity per unit area over the portion of the body which is both illuminated and visible:

$$\begin{aligned}\mathbf{I}(g) &= \int_{(i,v)} Y(i,e,g)\, dA \\ &= \int_{\Lambda=-\pi/2}^{(\pi/2)-g} \int_{L=-\pi/2}^{\pi/2} Jr(\Lambda, L, g) \\ &\qquad \cos eR^2 \cos L dL d\Lambda \\ &= 4JR^2 \int_{\Lambda=-\pi/2}^{-g/2} \int_{L=0}^{\pi/2} r(\Lambda, L, g) \\ &\qquad \cos\Lambda \cos^2 L dL d\Lambda, \quad (59)\end{aligned}$$

where the last equation follows from the fact that any bidirectional reflectance function r must be symmetric with respect to the northern and southern hemispheres and reciprocal with respect to the $\Lambda = -g/2$ meridian.

Equation (59) may be written in the form

$$\mathbf{I}(g) = JR^2 A_p(w, \bar{\theta}) \phi(g, w, \bar{\theta}), \quad (60)$$

where

$$A_p(w, \bar{\theta}) = \mathbf{I}(0)/JR^2 \quad (61a)$$

is the physical or geometric albedo, defined as the ratio of the brightness at zero phase to the brightness (J/π) (πR^2) of a Lambert disk of the same radius illuminated and viewed normally, and

$$\phi(g, w, \bar{\theta}) = \mathbf{I}(g)/\mathbf{I}(0) \quad (61b)$$

is the integral photometric function of the body. The integral phase function of a uniform planet is a symmetric function of g: $\phi(-g) = \phi(g)$.

In Hapke (1981) the reflectance of a macroscopically smooth, particulate surface, Eq. (53), was inserted into Eqs. (59)–(61) to give

$$\begin{aligned}A_p(w,0) &= (w/8)[(1 + B_0)P(0) - 1] \\ &\quad + (r_0/2)(1 + r_0/3), \quad (62)\end{aligned}$$

and

$$\begin{aligned}\phi(g, w, 0) = \frac{1}{A_p}\Bigg[&\left\{\frac{w}{8}[(1 + B(g)P(g) - 1]\right. \\ &\left. + \frac{r_0}{2}(1 - r_0)\right\}\{1 - \sin(|g|/2) \\ &\tan(|g|/2) \ln(\cot(|g|/4)\} + \frac{2}{3} r_0^2 \\ &\frac{\sin|g| + (\pi - |g|)\cos|g|}{\pi}\Bigg] \quad (63)\end{aligned}$$

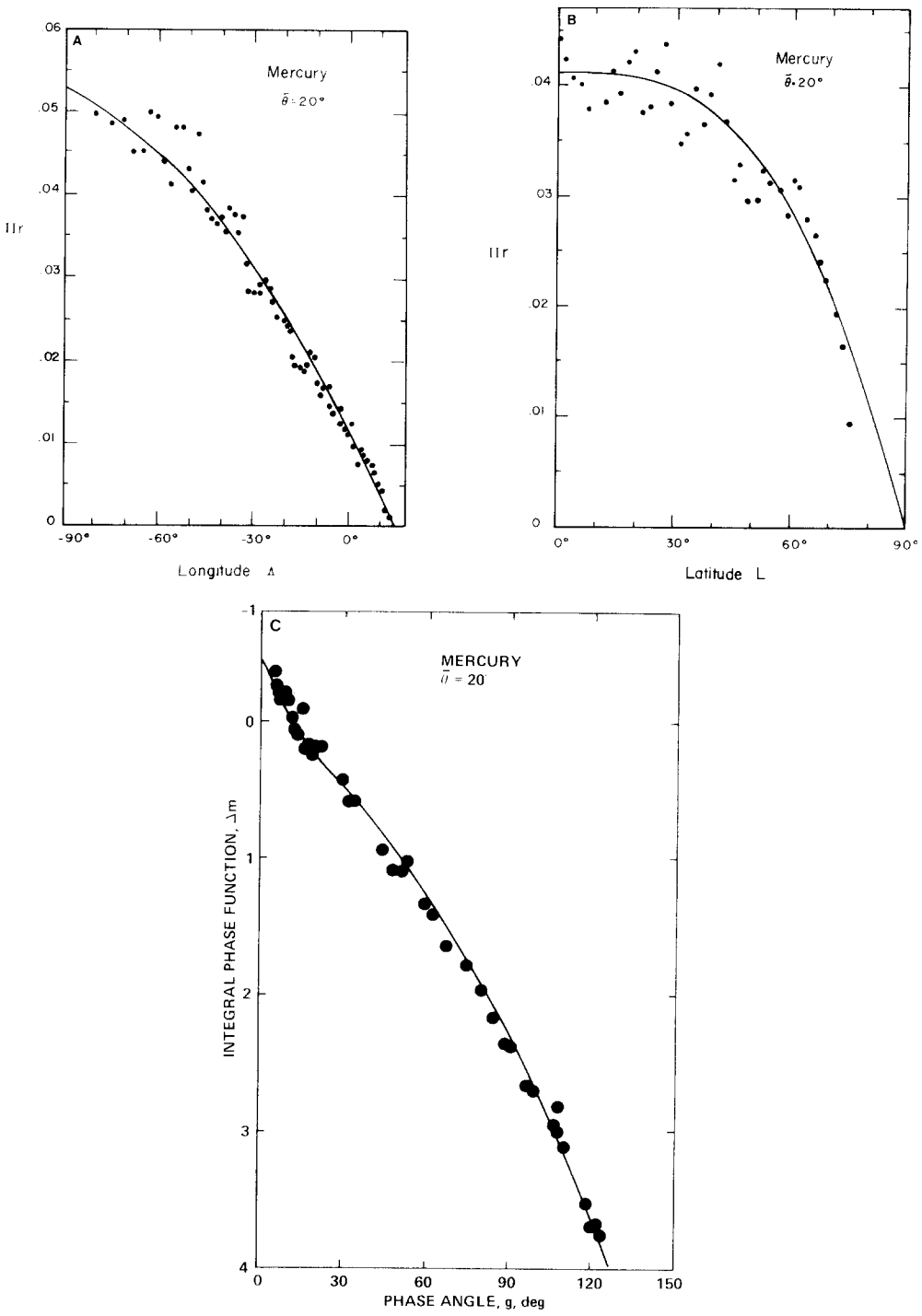

FIG. 5. Comparison of the theoretical photometric function with observations of Mercury. Lines are theoretical brightnesses calculated from the equations given in Sections V and VI with the following parameters: $w = 0.25$, $h = 0.40$, $\bar{\theta} = 20°$, and $P(g) = 1 + 0.579P_1 + 0.367P_2$, where P_1 and P_2 are the first and second Legendre polynomials, respectively. (A) Brightness versus longitude along the luminance equator at $g = 77°$. Dots are data of Mariner 10. (B) Brightness versus latitude along the $\Lambda = -50°$ meridian of luminance longitude at $g = 77°$. Dots are data of Mariner 10. (C) Integral phase function in magnitudes normalized to observations at $g = 10°$. Dots are data of Danjon (1949).

where

$$r_0 = [1 - (1 - w)^{1/2}]/[1 + (1 - w)^{1/2}] \quad (64)$$

is the bihemispherical reflectance of a semi-infinite medium of isotropic scatterers with single-scattering albedo w. In deriving (62) and (63) terms of order $r_0^3/24$ were ignored. The first term in (63) describes primarily the once-scattered light, and is proportional to the integral phase function of a sphere with Lommel–Seeliger surface elements. The second term arises from the multiply-scattered light and is proportional to the integral phase function of a sphere with Lambert surface elements.

When Eqs. (57) and (58) for a macroscopically rough surface were inserted into the above equations, analytic expressions for the physical albedo and integral phase function could not be obtained. Hence, the integration was done numerically for values of $\bar{\theta}$ up to 60°. The calculations showed that the integral photometric function of a rough-surfaced planet can be written in the form

$$A_p(w,\bar{\theta}) = (w/8)[(1 + B_0)P(0) - 1] + C(w,\bar{\theta})(r_0/2)(1 + r_0/3), \quad (65)$$

and

$$\phi(g,w,\bar{\theta}) = K(g,\bar{\theta})\phi(g,w,0), \quad (66)$$

where $\phi(g,w,0)$ is given by (63). The functions $C(w,\bar{\theta})$ and $K(g,\bar{\theta})$ are the calculated factors by which the physical albedo and integral phase function of a smooth-surfaced planet must be corrected for effects of macroscopic roughness. They are discussed below and shown in Figs. 6 and 7; K is tabulated in Table 1.

It was found that, to within 1%, C in (65) could be represented by the empirical expression

$$C(w,\bar{\theta}) = 1 - (0.048\bar{\theta} + 0.0041\bar{\theta}^2)r_0 - (0.33\bar{\theta} - 0.0049\bar{\theta}^2)r_0^2, \quad (67)$$

where $\bar{\theta}$ is in radians.

The factor $K(g,\bar{\theta})$ is controlled primarily by the shadowing function $S(i,e,g)$. Thus, within a small error, the phase function correction is the same for both the singly- and multiply-scattered components of ϕ and is insensitive to w. Hence, for practical calculations $K(g,\bar{\theta})$ can be taken as a function which is independent of w and multiplies both components of ϕ. It was found that for $g \lesssim 60°$, K could be represented to a good approximation by the empirical function

$$K(g,\bar{\theta}) = \exp\{-0.32\bar{\theta}[\tan\bar{\theta}\tan(g/2)]^{1/2} - 0.52\bar{\theta}\tan\bar{\theta}\tan(g/2)\}, \quad (68)$$

where $\bar{\theta}$ is in radians. For $g \gtrsim 60°$, this equation overestimates K, which should be found by interpolation using Table 1.

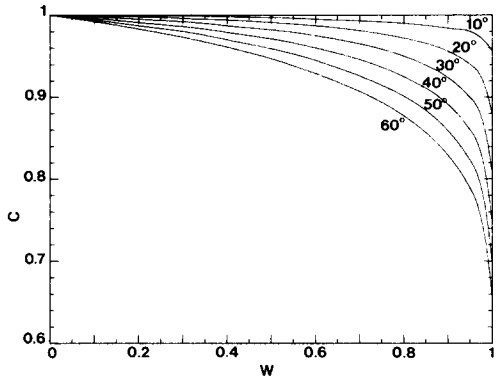

FIG. 6. The physical albedo correction factor $C(w,\bar{\theta})$ (Eq. 65) plotted against single-scattering albedo w for several values of mean slope $\bar{\theta}$.

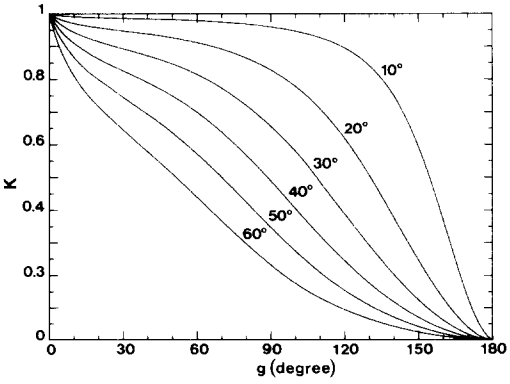

FIG. 7. The integral photometric function correction factor $K(g,\bar{\theta})$ (Eq. 66) versus phase angle g for several values of mean slope $\bar{\theta}$. This quantity is the ratio of the integral brightness of a planet with a rough surface to that of one with a macroscopically smooth surface.

TABLE I

INTEGRAL PHASE FUNCTION ROUGHNESS CORRECTION FACTORS $K(g,\bar{\theta})$

g (°)	$\bar{\theta}$						
	0°	10°	20°	30°	40°	50°	60°
0	1.00	1.00	1.00	1.00	1.00	1.00	1.00
2	1.00	0.997	0.991	0.984	0.974	0.961	0.943
5	1.00	0.994	0.981	0.965	0.944	0.918	0.881
10	1.00	0.991	0.970	0.943	0.909	0.866	0.809
20	1.00	0.988	0.957	0.914	0.861	0.797	0.715
30	1.00	0.986	0.947	0.892	0.825	0.744	0.644
40	1.00	0.984	0.938	0.871	0.789	0.692	0.577
50	1.00	0.982	0.926	0.846	0.748	0.635	0.509
60	1.00	0.979	0.911	0.814	0.698	0.570	0.438
70	1.00	0.974	0.891	0.772	0.637	0.499	0.366
80	1.00	0.968	0.864	0.719	0.566	0.423	0.296
90	1.00	0.959	0.827	0.654	0.487	0.346	0.231
100	1.00	0.946	0.777	0.575	0.403	0.273	0.175
110	1.00	0.926	0.708	0.484	0.320	0.208	0.130
120	1.00	0.894	0.617	0.386	0.243	0.153	0.0936
130	1.00	0.840	0.503	0.290	0.175	0.107	0.064
140	1.00	0.747	0.374	0.201	0.117	0.070	0.041
150	1.00	0.590	0.244	0.123	0.069	0.040	0.023
160	1.00	0.366	0.127	0.060	0.032	0.018	0.010
170	1.00	0.128	0.037	0.016	0.0085	0.0047	0.0026
180	1.00	0	0	0	0	0	0

Inspection of Fig. 7 shows that, although macroscopic roughness causes an opposition effect, the brightness peak is quite broad and cannot be separated from the rest of the phase curve. At small phase angles the regions which are appreciably shadowed tend to be close to the limb, where their effects on **I** are minimized by the factor cos e in the integrand of (59). Over most of the disk, as the Sun elevation angle changes, decreases in the brightnesses of those facets oriented away from the Sun are compensated by increases in the brightnesses of other facets which are oriented more directly toward the Sun. The major effect on ϕ occurs when $|g| > \pi/2$ and the heavily shadowed areas are nearer to the center of the disk. At very large phase angles the brightness of a rough planet is only a few percent of that of a body with a smooth surface, thus accounting for the fact, known since antiquity, that the Moon is invisible when less than about one day from new.

The theoretical integral phase function is compared with observations of Mercury by Danjon (1949) in Fig. 5C.

VII. CONCLUSIONS

The derivation of a planetary photometric function which was begun in Hapke (1981) is completed by equations (57), (58), (65), and (66). These sets of equations describe the scattering of light from a rough planetary regolith or undulating cloud top. The model is based on radiative transfer theory in a particulate medium and includes effects of microscopic interparticle shadowing, multiple scattering, and macroscopic roughness. The differential photometric equations for smooth and rough surfaces and the integral smooth-surfaced expressions are given in closed analytic form. The roughness correction factors for integral photometry are given by analytic functions for small phase angles, and for large phase angles may be obtained by interpolation using tabulated values. These equations should be useful in the interpretation of photometry of solar system objects when the scattering by an atmosphere is negligible or, for planets with optically thick atmospheres, when the scale heights of the gases and cloud particles are the same within the region of the atmosphere which contributes significantly to the brightness.

ACKNOWLEDGMENTS

I thank Karen Wells for assisting with the numerical integrations of Section VI, Eddie Wells for helpful comments and discussions, and Jay Goguen for useful criticisms and suggestions. This work was partially supported by a grant from the Planetary Geology Program of the National Aeronautics and Space Administration. During 1982–1983 I was a National Research Council–National Academy of Sciences Fellow at the Space Science Division, NASA Ames Research Center; major revisions to this work were done during this period.

REFERENCES

CHANDRASEKHAR, S. (1960). *Radiative Transfer*. Dover, New York.

COOK, A. (1981). A new photometric function for surfaces without atmospheres. Preprint.

COX, C., AND W. MUNK (1954). Measurement of the roughness of the sea surface from photographs of the Sun's glitter. *J. Opt. Soc. Amer.* **44**, 838–850.

DANJON, A. (1949). Photometrie et colorimetrie des planets mercure et Venus. *Bull. Astron.* **14,** 315–345.

HAGFORS, T. (1968). Relations between rough surfaces and their scattering properties as applied to radar astronomy. In *Radar Astronomy* (J. Evans and T. Hagfors, Eds.), pp. 187–218. McGraw–Hill, New York.

HAMEEN-ANTTILA, K. (1967). Surface photometry of the planet Mercury. *Ann. Acad. Sci. Fenn. Ser. A6* **252,** 1–19.

HAPKE, B. (1963). A theoretical photometric function for the lunar surface. *J. Geophys. Res.* **68,** 4571–4586.

HAPKE, B. (1966). An improved lunar theoretical photometric function. *Astron. J.* **71,** 333–339.

HAPKE, B. (1977). Interpretations of optical observations of Mercury and the Moon. *Phys. Earth Planet. Inter.* **15,** 264–274.

HAPKE, B. (1981). Bidirectional reflectance spectroscopy: 1. Theory. *J. Geophys. Res.* **86,** 3039–3054.

HAPKE, B. (1982). The Lumme–Bowell photometric parameters: Reality or fantasy? *Bull. Amer. Astron. Soc.* **14,** 726.

HAPKE, B., AND E. WELLS (1981). Bidirectional reflectance spectroscopy: 2. Experiments and observations. *J. Geophys. Res.* **86,** 3055–3060.

LUMME, K., AND E. BOWELL (1981a). Radiative transfer in the surfaces of atmosphereless bodies: I. Theory. *Astron. J.* **86,** 1694–1704.

LUMME, K., AND E. BOWELL (1981b). Radiative transfer in the surfaces of atmosphereless bodies: II. Interpretation of phase curves. *Astron. J.* **86,** 1705–1721.

MINNAERT, M. (1961). Photometry of the Moon. In *Planets and Satellites* (G. Kuiper and B. Middleurst, Eds.), pp. 213–248. Univ. of Chicago Press, Chicago.

MUHLEMAN, D. (1964). Radar scattering from Venus and the Moon. *Astron. J.* **69,** 34–41.

SAUNDERS, P. (1967). Shadowing on the ocean and the existence of the horizon. *J. Geophys. Res.* **72,** 4643–4649.

VAN DIGGELEN, J. (1959). Photometric properties of lunar crater floors. *Rech. Obs. Utrecht.* **14,** 1–114.

WAGNER, R. (1967). Shadowing of randomly rough surfaces. *J. Acoust. Soc. Amer.* **41,** 138–147.